THE ASTROPHYSICAL JOURNAL, 625:L23–L26, 2005 May 20

SWIFT OBSERVATIONS OF GRB 050128: THE EARLY X-RAY AFTERGLOW

S. CAMPANA,[1] L. A. ANTONELLI,[2] G. CHINCARINI,[1,3] S. COVINO,[1] G. CUSUMANO,[4] D. MALESANI,[5] V. MANGANO,[4] A. MORETTI,[1] C. PAGANI,[1,6] P. ROMANO,[1] G. TAGLIAFERRI,[1] M. CAPALBI,[7] M. PERRI,[7] P. GIOMMI,[7] L. ANGELINI,[8,9] P. BOYD,[8] D. N. BURROWS,[6] J. E. HILL,[6] C. GRONWALL,[6] J. A. KENNEA,[6] S. KOBAYASHI,[6,10] P. KUMAR,[11] P. MÉSZÁROS,[6] J. A. NOUSEK,[6] P. W. A. ROMING,[6] B. ZHANG,[12] A. F. ABBEY,[13] A. P. BEARDMORE,[13] A. BREEVELD,[14] M. R. GOAD,[13] O. GODET,[13] K. O. MASON,[14] J. P. OSBORNE,[13] K. L. PAGE,[13] T. POOLE,[13] AND N. GEHRELS[8]

Received 2005 March 24; accepted 2005 April 12; published 2005 April 28

ABSTRACT

Swift discovered GRB 050128 with the Burst Alert Telescope and promptly pointed its narrow field instruments to monitor the afterglow. X-ray observations started 108 s after the trigger time. The early decay of the afterglow is relatively flat, with a temporal decay modeled with a power-law index of ~ -0.3. A steepening occurs at later times ($\sim$1500 s) with a power-law index of ~ -1.3. During this transition, the observed X-ray spectrum does not change. We interpret this behavior as either an early jet break or evidence of a transition from the fast cooling regime to the slow cooling regime in a wind environment.

Subject headings: gamma rays: bursts — X-rays: individual (GRB 050128)

1. INTRODUCTION

The *Swift* gamma-ray burst mission (Gehrels et al. 2004) was successfully launched on 2004 November 20. Thanks to its fast-pointing capabilities, *Swift* is performing the first comprehensive observations of the early afterglow phase of gamma-ray bursts (GRBs). A few GRBs have been followed by *Swift* within 200 s from their trigger time: GRB 050117a (193 s), GRB 050126 (131 s), GRB 050128 (108 s), GRB 050215b (108 s), GRB 050219a (92 s), and GRB 050315 (83 s).

In this Letter we focus on GRB 050128. The Burst Alert Telescope (BAT; Barthelmy et al. 2005) on board *Swift* triggered and located GRB 050128 at 04:19:54 UT (Cummings et al. 2005). The burst profile is multipeaked with a T_{90} duration of 13.8 s. The fluence is 4.5×10^{-6} ergs cm^{-2} (15–350 keV), making it a "normal" burst with respect to the BATSE GRB population. The spectrum of the burst during the T_{90} interval can be described by a power-law model with a photon index $\Gamma = 1.5 \pm 0.1$ (15–350 keV). The peak energy is above 350 keV, making it a classical GRB.

Swift pointed autonomously to the GRB. We will report in the next sections about the XRT and UVOT observations. Ground-based follow-up observations started as soon as the GCN circular announcing the discovery of the new GRB was issued. This happened with some delay, since *Swift* was in the early phases of the mission and since each circular was being checked manually before being distributed. The first GCN circular on GRB 050128 was issued by the XRT team (Antonelli et al. 2005). The robotic 60 cm Rapid Eye Mount telescope located in La Silla pointed to GRB 050128 approximately 3 hr after the burst with good seeing conditions ($\sim 1''$). No new sources were discovered with an upper limit of $H > 17$ (Covino et al. 2005), $V > 18.2$, $R > 18.2$, or $I > 17.9$ (Melandri et al. 2005). A further upper limit came from the 2 m Faulkes Telescope South with $R > 20.5$ 11.5 hr after the burst (Monfardini et al. 2005). GRB 050128 has also been observed in the radio band at 8.4 GHz, yielding an upper limit of 100 μJy $\sim$11 days after the burst (Frail & Soderberg 2005).

In the following we focus on the observations by the X-Ray Telescope (XRT; Burrows et al. 2005a) on board *Swift*. In § 2 we describe the data analysis. In § 3 we discuss the theoretical implications of these observations, and in § 4 we draw our conclusions.

2. XRT AND UVOT OBSERVATIONS

UV/Optical Telescope (UVOT; Roming et al. 2005) observations started on 2005 January 28 at 20:03:07 UT, about 15.8 hr after the burst. This delay happened because UVOT was in safe mode at the trigger time. During each orbit UVOT acquired a single shot image in each filter, *U*, *B*, and *V*, in imaging mode. UVOT did not detect the afterglow. Upper limits on the first (summed over about 1 day elapsed time) UVOT observations are $V < 18.9$ ($V < 19.8$), $B < 20.3$ ($B < 21.1$), and $U < 19.2$ ($U < 20.3$).

XRT observed GRB 050128 after an automatic slew of the *Swift* satellite. However, XRT was not yet operating in its nominal automatic mode changing configuration but rather in a manual mode for the purpose of obtaining calibration data. Before pointing to GRB 050128, the XRT was observing a

[1] INAF–Osservatorio Astronomico di Brera, Via Bianchi 46, I-23807 Merate (LC), Italy; campana@merate.mi.astro.it.
[2] INAF–Osservatorio Astronomico di Roma, Via di Frascati 33, I-00040 Monteporzio, Italy.
[3] Università degli studi di Milano-Bicocca, Dipartimento di Fisica, Piazza delle Scienze 3, I-20126 Milan, Italy.
[4] INAF–Istituto di Astrofisica Spaziale e Fisica Cosmica Sezione di Palermo, Via Ugo La Malfa 153, I-90146 Palermo, Italy.
[5] International School for Advanced Studies (SISSA-ISAS), Via Beirut 2-4, I-34014 Trieste, Italy.
[6] Department of Astronomy and Astrophysics, 525 Davey Lab, Pennsylvania State University, University Park, PA 16802.
[7] ASI Science Data Center, Via Galileo Galilei, I-00044 Frascati (Rome), Italy.
[8] NASA/Goddard Space Flight Center, Greenbelt, MD 20771.
[9] Department of Physics and Astronomy, Johns Hopkins University, 3400 North Charles Street, Baltimore, MD 21218.
[10] Center for Gravitational Wave Physics, Pennsylvania State University, University Park, PA 16802.
[11] Department of Astronomy, University of Texas, RLM 15.308, Austin, TX 78712-1083.
[12] Department of Physics, University of Nevada, Box 454002, Las Vegas, NV 89154-4002.
[13] Department of Physics and Astronomy, University of Leicester, Leicester LE 1 7RH, UK.
[14] Mullard Space Science Laboratory, University College London, Holmbury St. Mary, Dorking, RH5 6NT Surrey, UK.

UVOT calibration target in photon counting mode (see Hill et al. 2004 for a description of XRT observing modes). XRT fully settled on the BAT position 108 s after the trigger. XRT observed GRB 050128 for 17 orbits following the first pointing, accumulating a nominal exposure time of 17,303 s (distributed over 73 ks). This low Earth orbit of *Swift* causes source observations to be interrupted each orbit. At the same time, thanks to the fast-pointing capability of *Swift*, several targets may be observed per orbit. At this early stage of the mission the analysis of the data is not straightforward. We analyzed the data by running the task *xrtpipeline* within FTOOLS version 5.3.1 and cutting out temporal intervals when the CCD temperature was higher than -50°C (see Burrows et al. 2005b) and when the total count rate in the 0.2–10 keV energy band over the entire CCD was larger than 85 counts s^{-1} (these counts are mainly soft counts and are due either to a dark current or to the bright Earth limb near the end of each snapshot observation). With these cuts we obtain a total exposure time of 13,047 s distributed over 11 orbits.

2.1. *Angular Analysis*

A fading source is clearly evident in all the XRT orbits. In the first two orbits the source is clearly piled up, and to derive an unbiased position we rely on the remaining ~10 ks exposure. An image has been extracted in the 0.5–10 keV energy band to avoid contamination from low-energy photons. The source position has been derived with XIMAGE (ver. 4.2.1) using the *centroid* command: R.A. = $14^{h}38^{m}18\overset{s}{.}0$, decl. = $-34°45'55\overset{''}{.}9$ (J2000). The main contributors to the positional uncertainty are the uncalibrated satellite attitude and boresight, resulting in an ~6″ error radius (90% confidence level).

2.2. *Temporal Analysis*

In order to properly track the decay of the fading source we have to account for the piled-up core in the first two snapshot observations. To this aim we extracted photons from an annular region (inner and outer radii 4 and 30 pixels, respectively) on-source. This aperture was then applied to the rest of the observations, even when it was not needed. The light curve will have an underestimated normalization, but it will not be distorted by pileup. A background light curve has also been extracted from an annular region (inner and outer radii 80 and 120 pixels, respectively) centered on the same position and free of other sources and hot pixels. Figure 1 shows the background-subtracted light curve in the 0.2–10 keV energy band. The source is clearly fading. The decay light curve is not consistent with a single power law ($\chi^2_{\rm red} = 2.6$, with 35 degrees of freedom [dof] and a null hypothesis probability [nhp] of 7×10^{-7}), being flat at the beginning and steepening at later times. We also tried a single power law with a different initial time t_0, considered here as a free parameter. We can account in principle for the observed decay with $t_0 = -780 \pm 290$ s; however, this early time is not physically meaningful. A better description of the data is provided by two power laws (with indices α_1 and α_2) smoothly joined at a break time t_b to model the decay. The fit with this model is good ($\chi^2_{\rm red} = 0.7$ with 33 dof and 0.90 nhp), with $\alpha_1 = -0.27^{+0.10}_{-0.12}$, $\alpha_2 = -1.30^{+0.18}_{-0.13}$, and $t_b = 1472^{+300}_{-290}$ s (these errors are 90% for one interesting parameter, i.e., $\Delta\chi^2 = 2.71$, throughout the Letter).

2.3. *Spectral Analysis*

Given the large variability in the source count rate and the knowledge from the temporal analysis of the existence of a change in the decay slope, we extracted three spectra from our data, one from each of the first two snapshots and one for the rest of the observation (see Fig. 1). The first two spectra were extracted from the same annular region as for the temporal analysis. The last spectrum, since the source is much fainter, was extracted from a circular region on-source of 30 pixel radius. Exposure times are 286, 1653, and 10731 s, respectively. Data have been filtered for grades 0–4 (according to the *XMM-Newton* nomenclature, i.e., single and double pixel events[15]), since at this stage the response matrix for the standard 0–12 pixel event is not fully calibrated. Ancillary response files were generated with the task *xrtmkarf* within FTOOLS (ver. 5.3.1), accounting for the different extraction regions. Data were rebinned to have at least 20 counts per energy bin and to allow χ^2 fitting within XSPEC (ver. 11.3.1).

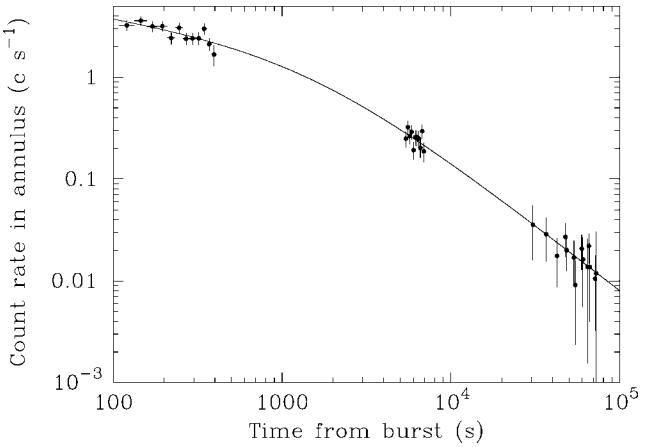

FIG. 1.—XRT 0.2–10 keV light curve extracted from an annular region centered on GRB 050128. The solid line represents the fit with two power laws smoothly joined. The conversion factor to translate the count rate into a 0.2–10 keV unabsorbed flux is 8.7×10^{-11} ergs cm^{-2} counts^{-1} (for a freely varying absorbed power-law model, see text).

We fit the data with an absorbed power-law model for all the observations. We first fixed the absorbing column density to the Galactic value of $N_{\rm H} = 4.8 \times 10^{20}$ cm^{-2}. We added a 5% systematic uncertainty to all our fits to account for the residuals still present in our response matrix (given the relatively low number of counts, this does not alter our results sensibly). This simple fit can account for the observed spectra. The fit is good with $\chi^2_{\rm red} = 1.1$ for 63 dof (0.21 nhp). The power-law photon index is $\Gamma = 1.66^{+0.06}_{-0.07}$. The 0.2–10 keV unabsorbed fluxes of the three observations with mid-times of 258 s, 6156 s, and 51587 s are 2.2×10^{-10}, 1.9×10^{-11}, and 6.6×10^{-13} ergs s^{-1} cm^{-2}, respectively. Given the slope change in the light curve, we also untie the power-law photon index of the three observations (even if it is not required by the statistics). The three photon indices are 1.59 ± 0.08, 1.79 ± 0.11, and 1.59 ± 0.23, respectively. These values are consistent with each other, with a small deviation in the second snapshot. Although the fit is consistent with the Galactic column density, we let the column density value vary. The fit is improved with a $\chi^2_{\rm red} = 0.9$ (62 dof, 0.66 nhp; see Fig. 2), and the improvement is significant according to the *F*-test (probability 4×10^{-4}, even if we improved an already statistically good fit). In Figure 3, we show the contour plot of the column density versus power-law photon index. The fit obtained with the column density fixed to the Galactic value is outside the 3 σ boundary.

[15] See, e.g., the *XMM-Newton* User's Handbook at http://xmm.vilspa.esa.es/external/xmm_user_support/documentation/uhb/index.html.

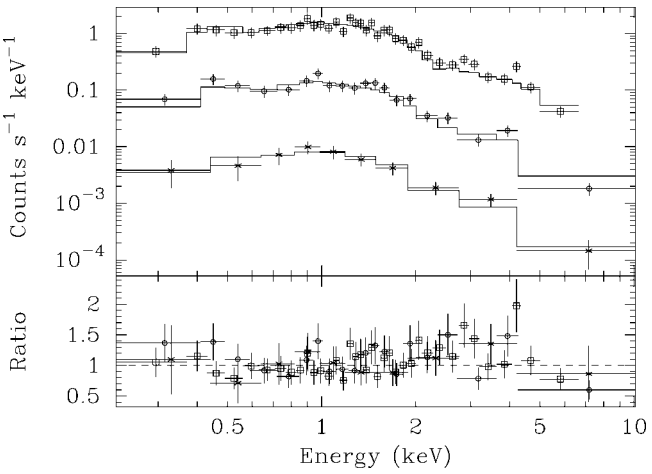

FIG. 2.—XRT 0.2–10 keV energy spectrum of GRB 050128. In the upper panel are plotted the spectra of the three snapshot observations described in the text (1: *squares*, 2: *circles*, other: *asterisks*) fit with an (freely) absorbed power law model. In the lower panel are the residuals from the same power-law fit to all the data.

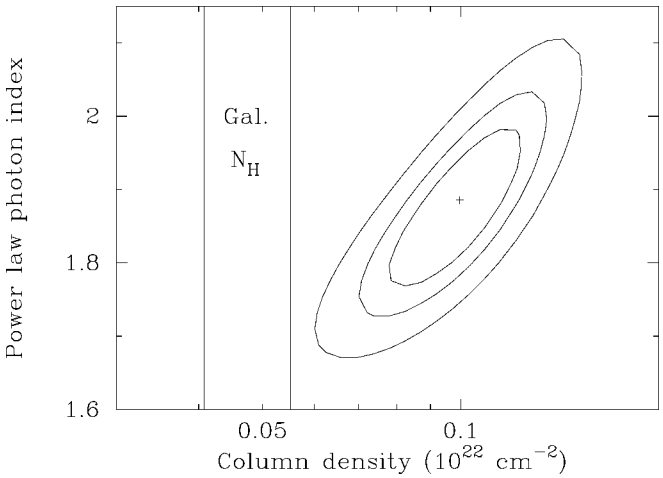

FIG. 3.—Contour plot of the column density vs. the power-law photon index for the X-ray spectrum of GRB 050128. Contours refer to the 1, 2, and 3 σ confidence levels. At the left of the contour plot the Galactic column density interval is centered on the value of 4.8×10^{20} cm^{-2}, with a 15% uncertainty.

The absorbing column density is $(1.0 \pm 0.2) \times 10^{21}$ cm^{-2}, and the power-law photon index $\Gamma = 1.88 \pm 0.12$. Unabsorbed fluxes (0.2–10 keV) are 2.4×10^{-10}, 2.0×10^{-11}, and 7.0×10^{-13} ergs s^{-1} cm^{-2}, respectively. Also, in this case, by leaving free the photon index to vary within the observations, the second one is characterized by a slightly steeper index.

3. PHYSICAL INTERPRETATIONS

The major result of the GRB 050128 afterglow concerns the monitoring in the X-ray band of its early temporal decay. This decay cannot be described by a simple power law but can be accounted for by a slowly varying double–power-law decay. During this transition there are no apparent marked spectral changes. The most straightforward interpretation is that the temporal break reveals a jet, i.e., corresponding to the epoch when the relativistic beaming angle ($1/\gamma$) becomes larger than the physical opening angle (θ_j) of the jet during the fireball deceleration (e.g., Rhoads 1999). In the slow cooling regime, for a uniform density circumstellar medium, the temporal decay changes from $t^{3(1-p)/4}$ to $\sim t^{-p}$ (e.g., Rhoads 1999), which is well consistent with the observed temporal decay indices when $p \sim 1.3$ is adopted. In such a case no spectral change is expected. However, the expected spectral photon index should be $-(p+1)/2 \sim -1.15$, too small to be compared with the observed value. In order to make the jet model work, one needs to assume $\nu_c < \nu_X < \nu_m$ before the jet break and $\nu_X > \max(\nu_c, \nu_m)$ after the jet break (here ν_m and ν_c are the typical synchrotron frequency and the cooling frequency, respectively). In such a case, $p \sim 1.3$ gives a consistent interpretation of both spectral and temporal indices in all three epochs, regardless of whether the medium is an interstellar medium (ISM) or a wind from a massive companion. This model requires a little bit of coincidence in that the synchrotron frequency happens to cross the X-ray band during the jet break. However, considering the rapid decline with time of ν_m, this is not a very unlikely possibility. Another caveat is that a flat electron spectrum $p \sim 1.3$ is abnormal in late afterglow fits (e.g., Panaitescu & Kumar 2001). However, since we are observing a previously unexplored early epoch, a small p required for the jet model to work cannot be ruled out. Possible ways to generate a flat electron spectrum have been suggested earlier (e.g., Bykov & Mészáros 1996). If this is indeed a jet break, this would be the earliest jet break detection so far. Using the standard definition of jet break time [i.e., $\theta_j = 1/\gamma(t_j)$], one can derive $\theta_0 = 1.^\circ8(t_j/2000\ \mathrm{s})^{3/8}(E_{52}/n)^{-1/8}[(1+z)/2]^{-3/8}$ for a constant density ISM and $\theta_0 = 3.^\circ7(t_j/2000\ \mathrm{s})^{1/4}(E_{52}/A_*)^{-1/4}[(1+z)/2]^{-1/4}$ for a wind model. Here n is the density of the ISM, E_{52} is the isotropic-equivalent burst energy in units of 10^{52} ergs, and $A = M/(4\pi v)$ is the wind parameter, with M being the mass-loss rate, v being the wind velocity, and $A_* = A/(5 \times 10^{11}\ \mathrm{g\ cm^{-1}})$. These jets are not extremely narrow (e.g., Covino et al. 2003) but are narrower than the typical jets identified in the previous late afterglow observations (e.g., Table 2 of Bloom et al. 2003). According to the GRB standard energy argument (e.g., Frail et al. 2001; Panaitescu & Kumar 2001), such a narrow jet should correspond to large isotropic gamma-ray energy. Since this burst was not particularly bright, it might lie in the low-energy tail of GRB-energy distribution, thus being another outlier for the standard energy relation.

Besides the jet interpretation, one could search for other possible solutions by considering the temporal and spectral relations in various afterglow models (e.g., Mészáros et al. 1998; Sari et al. 1998; Chevalier & Li 2000; Zhang & Mészáros 2004). The most straightforward model is within the framework of the standard isotropic wind model (Chevalier & Li 2000). The first cluster of the data corresponds to the $\nu_c < \nu_X < \nu_m$ regime, in which the temporal index $-1/4$ and the photon spectral index $-3/2$ are expected. The second and the third clusters of the data correspond to the regime of $\nu_m < \nu_X < \nu_c$, in which the temporal index $-(3p-1)/4$ and the photon spectral index $-1-(p-1)/2$ are expected. All these are consistent with the data for $p \sim 2.1$. In this interpretation, one needs to assume that both ν_m and ν_c cross the X-ray band during the gap between the first two clusters of data and that the frequencies switch the order. This could be achieved with a small wind parameter (e.g., A_* in the range of 0.01–0.001). One caveat is that in the wind model $\nu_c \propto t^{1/2}$, so that the time interval of the gap is not long enough for ν_c to completely cross the band. Nonetheless, the spectral slope in the second cluster is slightly steeper than the other two, which might be still consistent with the data if one introduces an evolving cooling break near the high-energy edge of the band during the epoch of the second snapshot. Introducing a slightly steeper density profile (larger than r^{-2} for the wind case) could further alleviate the problem. Furthermore, if the electron equipartition factor ϵ_B drops during

the temporal gap, this would speed up the ν_c crossing timescale, making the model more consistent with the data.

Finally, we note also that a similar behavior has been observed in the optical light curve of GRB 021004, even if with a slightly longer break time (~0.1 days; Fox et al. 2003). This transition has been interpreted by Li & Chevalier (2003) as a fast to slow cooling transition.

4. CONCLUSION

Swift is exploring for the first time the early stages of GRB afterglow decays. We detect a clear early temporal break in the X-ray afterglow of GRB 050128, with the spectral indices not changing around the break. It could be argued that the data are consistent with either a jet model or a wind model. The jet model requires a flat electron spectrum and an assumed spectral domain change within the temporal gap between the first two snapshot observations. If this is true, we may have detected the earliest jet break so far. The wind model requires a (relatively) low ambient density and possibly an evolution of the ϵ_B parameter. We note that in this last case, passages from fast to slow cooling regimes might have remained hidden in the great majority of GRB afterglows if they are characterized by such a tenuous environment, due to the late times at which they were observed.

The early detection of the X-ray afterglow, coupled with the initial flat decay, allows us to estimate its fluence $\mathcal{F} = \int F(t)dt$. In fact, given the values of α_1 and α_2, $\mathcal{F}$ is not very sensitive to the start time t_0 of the afterglow and is dominated by the flux at the break time t_b. The fluence between 108 and 73,000 s is $(7 \pm 2) \times 10^{-7}$ ergs cm^{-2} (15–350 keV), while extrapolating from $t = 0$ to $+\infty$ it is $\mathcal{F} = 9^{+5}_{-3} \times 10^{-7}$ ergs cm^{-2}. These values amount to 15% and 20% of the prompt fluence in the same energy band, respectively. Since prompt and afterglow spectra are similar, we might expect a relatively small difference in the bolometric correction. This is the first determination of the ratio between GRB proper and early afterglow energetics.

This work is supported at OAB by funding from ASI of grant I/R/039/04, at Penn State by NASA contract NAS5-00136 and at the University of Leicester by PPARC of grants PPA/G/S/00524 and PPA/Z/S/2003/00507. We gratefully acknowledge the contributions of dozens of members of the XRT and UVOT team at OAB, PSU, UL, GSFC, ASDC, and MSSL and our subcontractors, who helped make this instrument possible.

REFERENCES

Antonelli, L. A., et al. 2005, GCN Circ. 2991, http://gcn.gcfs.nasa.gov/gcn/gcn3/2991.gcn3
Barthelmy, S. D., et al. 2005, Space Sci. Rev., in press
Bloom, J. S., Frail, D. A., & Kulkarni, S. R. 2003, ApJ, 594, 674
Burrows, D. N., et al. 2005a, Space Sci. Rev., in press
———. 2005b, ApJ, 622, L85
Bykov, A. M., & Mészáros, P. 1996, ApJ, 461, L37
Chevalier, R. A., & Li, Z. Y. 2000, ApJ, 536, 195
Covino, S., et al. 2003, A&A, 404, L5
———. 2005, GCN Circ. 2999, http://gcn.gcfs.nasa.gov/gcn/gcn3/2999.gcn3
Cummings, J., et al. 2005, GCN Circ. 2992, http://gcn.gcfs.nasa.gov/gcn/gcn3/2992.gcn3
Fox, D. W., et al. 2003, Nature, 422, 284
Frail, D. A., et al. 2001, ApJ, 562, L55
Frail, D. A., & Soderberg, A. M. 2005, GCN Circ. 3011, http://gcn.gcfs.nasa.gov/gcn/gcn3/3011.gcn3
Gehrels, N., et al. 2004, ApJ, 611, 1005
Hill, J. E., et al. 2004, Proc. SPIE, 5165, 217
Li, Z., & Chevalier, R. A. 2003, ApJ, 589, L69
Melandri, A., et al. 2005, GCN Circ. 3004, http://gcn.gcfs.nasa.gov/gcn/gcn3/3004.gcn3
Mészáros, P., Rees, M. J., & Wijers, R. A. M. J. 1998, ApJ, 499, 301
Monfardini, A., et al. 2005, GCN Circ. 3001, http://gcn.gcfs.nasa.gov/gcn/gcn3/3001.gcn3
Panaitescu, A., & Kumar, P. 2001, ApJ, 560, L49
Rhoads, J. E. 1999, ApJ, 525, 737
Roming, P. W. A., et al. 2005, Space Sci. Rev., in press
Sari, R., Piran, T., & Narayan, R. 1998, ApJ, 497, L17
Zhang, B., & Mészáros, P. 2004, Int. J. Mod. Phys. A, 19, 2385